International Journal of Intelligent Unmanned Systems. 2016, Volume 4, Issue 1, 2016, pp. 43-66
DOI:10.1108/IJIUS-08-2015-0011

Fault Tolerant Control of a Quadrotor using $\mathcal{L}_1$ Adaptive Control

Dan Xu* James F Whidborne† Alastair Cooke‡

10 March 2016

Abstract

The growing use of small unmanned rotorcraft in civilian applications means that safe operation is increasingly important. Here, the fault tolerant properties to faults in the actuators of an $\mathcal{L}_1$ adaptive controller for a quadrotor vehicle are investigated. $\mathcal{L}_1$ adaptive control provides fast adaptation along with decoupling between adaptation and robustness. This makes the approach a suitable candidate for fault tolerant control of quadrotor and other multirotor vehicles. In the paper, the design of an $\mathcal{L}_1$ adaptive controller is presented and compared to a fixed-gain LQR controller. The $\mathcal{L}_1$ adaptive is shown to have improved performance when subject to actuator faults, and a higher range of actuator fault tolerance.

Keywords: $\mathcal{L}_1$ adaptive control, quadrotor control, fault tolerant control, LQR control, UAV control, rotor failure.

1 Introduction

Quadrotors (or quadcoptors) have become very popular platforms amongst hobbyists and research laboratories and are increasingly being used as observation platforms for a number of roles. The main reasons for this appears to be the mechanical simplicity (compared to traditional rotorcraft) which means very low cost. Despite lacking inherent stability, the simplicity also means the aircraft is relatively easy to control by automatic feedback, at least for non-aggressive manoeuvres in calm conditions. For example, Bouabdallah et al. [2004a] achieved satisfactory results for a PID controller. Using a quarternion description, the attitude can be controlled using just PD control [Tayebi and McGilvray, 2006]. More recently, PD control [Marks et al., 2012] has been shown in simulation to achieve good responses even for high upset angles. Satisfactory trajectory tracking and attitude control can be obtained with LQR control [Cowling et al., 2006, 2010, Rinaldi et al., 2013]. However, in order for quadrotors and similar unmanned vehicles to undertake many proposed roles, high levels of safety are required, but the lack of inherent stability means that the control system is required to be fault tolerant. In this paper we propose the use of an $\mathcal{L}_1$ adaptive controller to provide an increased tolerance to partial failure of the actuators/effectors.

The $\mathcal{L}_1$ adaptive controller was originally proposed in Cao and Hovakimyan [2006a], and developed through a series of papers [Cao and Hovakimyan, 2006b, 2007b,c, 2008a,b,c, 2009, Xargay et al., 2010]. Additional details of the method are given in Hovakimyan and Cao [2010]. The $\mathcal{L}_1$ adaptive control architecture guarantees stability robustness in the presence of fast adaptation, achieved via continuous feedback. An important feature of this architecture is the separation between estimation (adaptation) and control (robustness). This is achieved by an appropriate modification of the control objective and consideration of the fact that compensation for uncertainties in any feedback loop can be made only within the bandwidth of the control channel. The new objective is to track (both in transient and steady-state) the input and the output of an auxiliary linear closed-loop reference system. This allows the use of high gains inside the adaptation block, thus achieving fast adaptation rates which are beneficial for both performance and robustness. The trade-off between these is resolved through the selection of an appropriate filter structure, thus allowing transient tracking to be improved by increasing the adaptation rate without generating high-frequencies in the control signal.

The $\mathcal{L}_1$ adaptive control approach has been applied to many problem [Cao and Hovakimyan, 2009, Sarhadi et al., 2014, for example]. It has also been proposed for the control of quadrotors. Michini and How [2009]

*Flight Test Center, Commercial Aircraft Corporation of China Ltd, Shanghai, 200232, China. email:xudan1@comac.cc
†Centre for Aeronautics, Cranfield University, Bedfordshire MK45 0AL, UK. email:j.f.whidborne@cranfield.ac.uk
‡Centre for Aeronautics, Cranfield University, Bedfordshire MK45 0AL, UK. email:a.cooke@cranfield.ac.uk

presented a design procedure for $\mathcal{L}_1$ adaptive control output feedback control and demonstrated its potential by applying it to an indoor quadrotor helicopter. Flight test results demonstrate that the designer specifications correspond to the expected physical responses. Mallikarjunan et al. [2012] designed and implemented an $\mathcal{L}_1$ adaptive controller using a backstepping architecture. Three variations were flight tested, and the best results obtained for the variation that used a quarternion model description. De Monte and Lohmann [2013] [also see De Monte and Lohmann, 2014] also combine a backstepping approach with an $\mathcal{L}_1$ adaptive control to account for the time-varying nonlinear error dynamics that arise from the backstepping design. Verifiable bounds on the tracking error and input signals are provided. In Capello et al. [2013], a mixed deterministic-randomized approach for the control law design of an $\mathcal{L}_1$ adaptive controller is proposed. The controller is tested in simulation and shows good performance. An $\mathcal{L}_1$ adaptive controller is designed by Capello et al. [2012] and implemented on a test platform. Experiments show better response characteristics than a PD controller. Zuo and Ru [2014] proposed improving trajectory tracking for a quadrotor by combining feedforward control with $\mathcal{L}_1$ adaptive control. Bounds on the tracking error are given. Akkinapalli et al. [2014] presented a quaternion-based backstepping controller for a hexarotor that uses $\mathcal{L}_1$ adaptive augmentation for robust attitude tracking.

The question of tolerance to failure of a quadrotor actuator/effector has been addressed previously. Maintaining hover while losing control of one degree-of-freedom (notably yaw) is an approach considered by, for example, Mueller and D'Andrea [2015] [see also Mueller and D'Andrea, 2014] and by Lanzon et al. [2014]. Control allocation methods that use actuator redundancy in hexrotor or octorotor arrangements have been proposed by, for example, Adîr et al. [2011], Marks et al. [2012], Hamayun et al. [2015] and Alwi and Edwards [2015]. A number of approaches to partial actuator failure have been investigated. For example, a backstepping approach is described in Zhang et al. [2010], whilst a Lyapunov-based adaptive control strategy is investigated in Zhang and Zhang [2010]. A model reference adaptive control approach is described by Dydek et al. [2013], and an LPV model reference approach by Rotondo et al. [2015]. An approach that incorporates trajectory replanning is proposed by Chamseddine et al. [2015]. A review of these and some of the other approaches is provided by Zhang et al. [2013] and Zhang and Chamseddine [2012].

$\mathcal{L}_1$ adaptive control does not appear to have been explicitly investigated for its fault tolerant properties for quadrotors. Hence that is the theme of this paper. In the next section, the quadrotor model is described. In Section 3, $\mathcal{L}_1$ adaptive control is summarized. Section 4 describes the $\mathcal{L}_1$ adaptive controller design. In addition, a fixed-gain LQR controller with integral action is described. Simulations were performed for the vehicle when subjected to actuator faults, some of the results are presented in Section 5, and the results for the two controllers compared. Finally some conclusions are drawn.

2 Quadrotor Model

Dynamic modelling of small VTOL UAVs has been well covered in many sources. In this research, the Newton-Euler approach is used [Bouabdallah et al., 2004b, Mian and Wang, 2008, Michini et al., 2011, for example] with the following assumptions:

- the structure is rigid and symmetric,
- the propellers are rigid,
- the rotor thrust and the drag are proportional to the square of the speed of the rotor,
- the rotor axes are parallel and lie in the z direction,
- ground effect is neglected,
- the inertia matrix is diagonal,
- the rotor Coriolis force and wind forces are not included,
- and the motor dynamics are ignored.

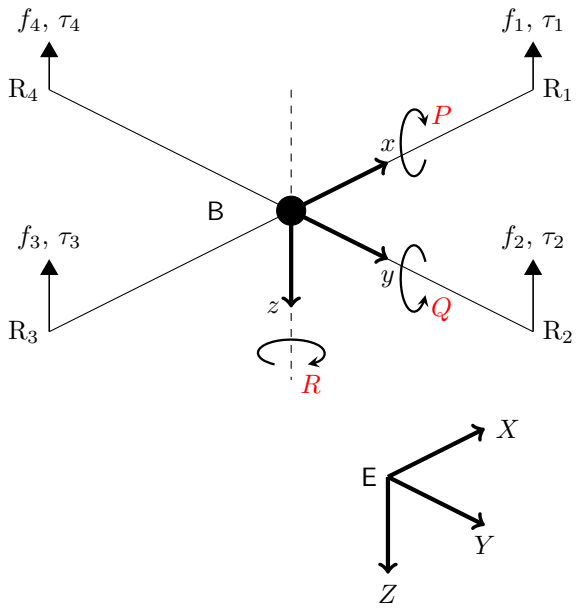

Figure 1: Quadrotor schematic

The basic vehicle configuration, Earth frame, E, and body frame, B, are shown in Figure 1. The body frame has the axes originating at the center of mass of the vehicle. An inertial coordinate frame is fixed to the Earth and has axes in the conventional North-East-Down arrangement. It is assumed that the Earth is flat and stationary. Each rotor provides a thrust force, f_i, and torque, τ_i. These combine to a vector of moments about the body axis, $\mathbf{M} = [L, M, N]^T$ and a thrust force in the negative z direction, $-T$.

The orthogonal rotation matrix $\mathbf{S}_b$ to transform from body frame to Earth frame is [Cook, 2013]

$$\mathbf{S}_b = \begin{bmatrix} c_\theta c_\psi & c_\theta s_\psi & -s_\theta \\ s_\phi s_\theta c_\psi - c_\phi s_\psi & c_\phi c_\psi + s_\phi s_\theta s_\psi & c_\theta s_\phi \\ c_\phi s_\theta c_\psi + s_\phi s_\psi & c_\phi s_\theta s_\psi - s_\phi c_\psi & c_\theta c_\phi \end{bmatrix} \tag{1}$$

where c_θ denotes $\cos\theta$, s_θ denotes $\sin\theta$, etc and (ϕ, θ, ψ) is the standard Euler angle roll-pitch-yaw triplet.

The gravitational force vector, $\mathbf{F}_g$, in the body axis is

$$\mathbf{F}_g = m\,\mathbf{S}_b \begin{bmatrix} 0 \\ 0 \\ g \end{bmatrix} = mg \begin{bmatrix} -s_\theta \\ c_\theta s_\phi \\ c_\theta c_\phi \end{bmatrix}. \tag{2}$$

where g is gravitational field constant which is taken as $g = 9.81\text{N kg}^{-1}$.

The Newton-Euler equations of motion of the body axes frame are

$$\mathbf{F} = m\dot{\mathbf{V}} + \boldsymbol{\omega} \times m\mathbf{V}, \tag{3}$$

$$\mathbf{M} = \mathbf{I}\dot{\boldsymbol{\omega}} + \boldsymbol{\omega} \times \mathbf{I}\boldsymbol{\omega} \tag{4}$$

where $\mathbf{V} = [U, V, W]^T$ is the vector of velocities in the body frame, $\boldsymbol{\omega} = [P, Q, R]^T$ is the vector of angular rates in the body frame, $\mathbf{I} = \text{diag}(I_x, I_y, I_z)$ is the moments of inertia matrix, m is the mass of the vehicle, $\mathbf{F} = \mathbf{F}_g + [0, 0, -T]^T$ is the vector of the forces acting on the center of mass, and $\mathbf{M} = [L, M, N]^T$ is the vector of moments acting about the center of mass.

Expanding and rearranging (3) gives

$$\begin{bmatrix} \dot{U} \\ \dot{V} \\ \dot{W} \end{bmatrix} = \frac{1}{m} \begin{bmatrix} 0 \\ 0 \\ -T \end{bmatrix} + g \begin{bmatrix} -s_\theta \\ c_\theta s_\phi \\ c_\theta c_\phi \end{bmatrix} - \begin{bmatrix} QW - RV \\ RU - PW \\ PV - QU \end{bmatrix}. \tag{5}$$

Similarly expanding and rearranging (4) gives

$$\begin{bmatrix}\dot{P}\\ \dot{Q}\\ \dot{R}\end{bmatrix} = \begin{bmatrix}\frac{L}{I_x}\\ \frac{M}{I_y}\\ \frac{N}{I_z}\end{bmatrix} - \begin{bmatrix}\frac{I_z-I_y}{I_x}QR\\ \frac{I_x-I_z}{I_y}RP\\ \frac{I_y-I_x}{I_z}PQ\end{bmatrix}. \tag{6}$$

The rotation matrix, $\mathbf{S}_b$, from (1) is used to express the movement of the vehicle in the Earth axes once the body-centric velocities are known:

$$\begin{bmatrix}\dot{X}\\ \dot{Y}\\ \dot{Z}\end{bmatrix} = \mathbf{S}_b^T \begin{bmatrix}U\\ V\\ W\end{bmatrix} \tag{7}$$

$$= \begin{bmatrix}c_\psi c_\theta & c_\psi s_\theta s_\phi - s_\psi c_\phi & c_\psi s_\theta c_\phi + s_\psi s_\phi\\ s_\psi c_\theta & s_\psi s_\theta s_\phi + c_\psi c_\phi & s_\psi s_\theta c_\phi - c_\psi s_\phi\\ -s_\theta & c_\theta s_\phi & c_\theta c_\phi\end{bmatrix} \begin{bmatrix}U\\ V\\ W\end{bmatrix}. \tag{8}$$

The Euler angle rates are related to the body angle rates through

$$\begin{bmatrix}P\\ Q\\ R\end{bmatrix} = \begin{bmatrix}1 & 0 & -s_\theta\\ 0 & c_\phi & s_\phi c_\theta\\ 0 & -s_\phi & c_\theta c_\phi\end{bmatrix} \begin{bmatrix}\dot{\phi}\\ \dot{\theta}\\ \dot{\psi}\end{bmatrix}, \tag{9}$$

giving

$$\begin{bmatrix}\dot{\phi}\\ \dot{\theta}\\ \dot{\psi}\end{bmatrix} = \begin{bmatrix}1 & t_\theta s_\phi & t_\theta c_\phi\\ 0 & c_\phi & -s_\phi\\ 0 & \frac{s_\phi}{c_\theta} & \frac{c_\phi}{c_\theta}\end{bmatrix} \begin{bmatrix}P\\ Q\\ R\end{bmatrix}. \tag{10}$$

A general state space model, $\dot{\mathbf{x}} = f(\mathbf{x}, \mathbf{\Gamma})$, is obtained from (5), (6), (8) and (10) with state variables given by

$$\mathbf{x} = \begin{bmatrix}U & V & W & P & Q & R & X & Y & Z & \phi & \theta & \psi\end{bmatrix}^T, \tag{11}$$

and control given by

$$\mathbf{\Gamma} = \begin{bmatrix}T & L & M & N\end{bmatrix}^T. \tag{12}$$

The resulting model is

$$\frac{d}{dt}\begin{bmatrix}U\\ V\\ W\\ P\\ Q\\ R\\ X\\ Y\\ Z\\ \phi\\ \theta\\ \psi\end{bmatrix} = \begin{bmatrix}-g\ s_\theta - (QW - RV)\\ g\ c_\theta s_\phi - (RU - PW)\\ -\frac{T}{m} + g c_\theta c_\phi - (PV - QU)\\ \frac{L}{I_x} - \left(\frac{I_z-I_y}{I_x}\right)QR\\ \frac{M}{I_y} - \left(\frac{I_x-I_z}{I_y}\right)RP\\ \frac{N}{I_z} - \left(\frac{I_y-I_x}{I_z}\right)PQ\\ (c_\psi c_\theta)U + (c_\psi s_\theta s_\phi - s_\psi c_\phi)V + (c_\psi s_\theta c_\phi + s_\psi s_\phi)W\\ (s_\psi c_\theta)U + (s_\psi s_\theta s_\phi + c_\psi c_\phi)V + (s_\psi s_\theta c_\phi - c_\psi s_\phi)W\\ -s_\theta U + (c_\theta s_\phi)V + (c_\theta c_\phi)W\\ P + (t_\theta s_\phi)Q + (t_\theta c_\phi)R\\ c_\phi Q - s_\phi R\\ \left(\frac{s_\phi}{c_\psi}\right)Q + \left(\frac{c_\phi}{c_\theta}\right)R\end{bmatrix}. \tag{13}$$

2.1 Draganfly X-pro

The vehicle that is modelled for use in this work is the Draganfly X-pro quadrotor (developed by Draganfly Innovations Inc) shown in Figure 2. The quadrotor arm length is 0.50 m. Each rotor has two blades. The radius of the rotor is 0.258 m, and the mean chord of the blade is 0.032 m. A 14.8 V lithium-ion polymer

Figure 2: Draganfly X-pro

battery is used for supplying the electric power, this being the maximum voltage that can be supplied to a motor. A full model of the vehicle has been obtained by wind-tunnel and other experiments [Martínez, 2007]. The mass and inertia terms are

$$m = 2.356\,\text{kg}, \qquad I_x = 0.1676\,\text{kg m}^2, \tag{14}$$

$$I_y = 0.1676\,\text{kg m}^2, \qquad I_z = 0.29743\,\text{kg m}^2. \tag{15}$$

2.2 Actuator model

The control is effected by four actuators, each of which makes a contribution to the force and moment by means of a thrust vector, τ_i, $i = 1, \ldots, 4$, that acts in the $-z$ direction at the end of each arm as shown in Figure 1. The rotors are driven by voltages to four electronic motors, the thrust-voltage relationship can be expressed as [Martínez, 2007]

$$f_i = k_f {v_i}^2, \quad i = 1, 2, 3, 4 \tag{16}$$

where f_i is the individual thrust from ith rotor, v_i is the individual voltage input and $k_f = 0.11$ N/V^2 has been calculated from the experimental data presented in Martínez [2007].

The individual torque of each rotor is [Martínez, 2007]

$$\tau_i = k_\tau {v_i}^2 \tag{17}$$

where τ_i is the individual torque from ith rotor and $k_\tau = 0.052$ Nm/V^2 is calculated from the data in Martínez [2007]. The force and moments are not linear with voltage, but linear with squared voltage, therefore the squared voltages are used as the final full system model input vector, $\mathbf{U} = [v_1^2, v_2^2, v_3^2, v_4^2]^T$.

The total thrust force provided is the sum of the forces provided by each rotor. The roll and pitch moments are generated by differences between the respective pairs of rotors. The yaw moment is generated by the unbalanced torque of the four rotors. These are represented by a control allocation matrix, $\mathbf{\Lambda}$, such that

$$\mathbf{\Gamma} = \mathbf{\Lambda U} \tag{18}$$

where

$$\mathbf{\Lambda} = \begin{bmatrix} k_f & k_f & k_f & k_f \\ 0 & -lk_f & 0 & lk_f \\ lk_f & 0 & -lk_f & 0 \\ k_\tau & -k_\tau & k_\tau & -k_\tau \end{bmatrix}, \tag{19}$$

and l is the moment arm, which is 0.5 m [Martínez, 2007].

In order to simulate the actuator failure, a failure model is also needed. A matrix $\mathbf{\Delta}$ is defined as follow:

$$\mathbf{\Delta} = \text{diag}\begin{bmatrix}\delta_1 & \delta_2 & \delta_3 & \delta_4\end{bmatrix} \qquad \delta_i \in (0,1], \qquad i = 1,2,3,4 \tag{20}$$

where δ_i denotes the thrust/torque fraction after failure. For example, $\delta_1 = 0.6$, means rotor 1 lost 40% thrust/torque. Thus the full actuator model is:

$$\mathbf{\Gamma} = \mathbf{\Lambda}\mathbf{\Delta}\mathbf{U}. \tag{21}$$

3 $\mathcal{L}_1$ Adaptive Control

The approach to the $\mathcal{L}_1$ adaptive control taken here is to design an inner-loop state-feedback controller that stabilizes the quadrotor for the nominal design case. An output feedback $\mathcal{L}_1$ adaptive controller [Cao and Hovakimyan, 2007a] is then wrapped around the stable inner loop to provide adaptation for failure and modelling uncertainties; this follows the basic scheme of Michini and How [2009]. The approach was also used by Ene et al. [2013] for a high manoeuvrability aircraft.

3.1 $\mathcal{L}_1$ problem formulation

Consider the following MIMO nonlinear system with uncertainty input gain

$$\dot{\mathbf{x}}(t) = \mathbf{A}\mathbf{x}(t) + \mathbf{B}_m\mathbf{\Delta}(t)\mathbf{u}(t) + \mathbf{f}(t,\mathbf{x}(t)), \quad \mathbf{x}(0) = \mathbf{x}_0 \tag{22}$$

$$\mathbf{y}(t) = \mathbf{C}\mathbf{x}(t) \tag{23}$$

where $\mathbf{x}(t) \in \mathbb{R}^n$ is the measurable system state vector, $\mathbf{u}(t) \in \mathbb{R}^m$ is the control signal, $\mathbf{y}(t) \in \mathbb{R}^m$ is the regulated output, $\mathbf{A} \in \mathbb{R}^{n\times n}$ is known, $\mathbf{B}_m \in \mathbb{R}^{n\times m}$ and $\mathbf{C} \in \mathbb{R}^{m\times n}$ are known and constant, $(\mathbf{A},\mathbf{B})$ is controllable and $(\mathbf{A},\mathbf{C})$ is observable. Matrix $\mathbf{\Delta}(t) \in \mathbb{R}^{n\times n}$ consists of unknown time-varying parameters and $\mathbf{f} : \mathbb{R}\times\mathbb{R}^n \to \mathbb{R}^n$ is a vector of unknown nonlinear functions.

Now consider the control

$$\mathbf{u}(t) = \mathbf{u}_1(t) + \mathbf{u}_2(t). \tag{24}$$

An inner-loop controller $\mathbf{K}_1 \in \mathbb{R}^{m\times n}$ is designed so that $\mathbf{u}_1(t) = \mathbf{K}_1\mathbf{x}(t)$ and $\mathbf{A}_m = \mathbf{A} - \mathbf{B}_m\mathbf{K}_1$ is Hurwitz [Cao and Hovakimyan, 2008c]. The resulting system to be controlled by the adaptive control is

$$\dot{\mathbf{x}}(t) = \mathbf{A}_m\mathbf{x}(t) + \mathbf{B}_m\mathbf{\Delta}(t)\mathbf{u}_2(t) + \tilde{\mathbf{f}}(t,\mathbf{x}(t)), \quad \mathbf{x}(0) = \mathbf{x}_0 \tag{25}$$

$$\mathbf{y}(t) = \mathbf{C}\mathbf{x}(t) \tag{26}$$

with the control signal, $\mathbf{u}_2(t)$, generated by the adaptive controller and $\tilde{\mathbf{f}} : \mathbb{R}\times\mathbb{R}^n \to \mathbb{R}^n$ is a vector of unknown nonlinear functions that includes the $\mathbf{B}_m(I - \mathbf{\Delta}(t))\mathbf{u}_1(t)$ term.

3.2 $\mathcal{L}_1$ adaptive control architecture

Figure 3 shows the main structure of this architecture which includes a state predictor block, a fast adaptation block with projection-based adaptive laws, and the control law with a low-pass filter. The approach follows that proposed in Hovakimyan and Cao [2010, Section 3.2] where further detail is presented.

Assume that the function $\tilde{\mathbf{f}}(t,\mathbf{x}(t))$ that represents the uncertainties and disturbances has the following form

$$\tilde{\mathbf{f}}(t,\mathbf{x}(t)) = \mathbf{B}_m\mathbf{f}_1(t,\mathbf{x}(t)) + \mathbf{B}_{um}\mathbf{f}_2(t,\mathbf{x}(t)) \tag{27}$$

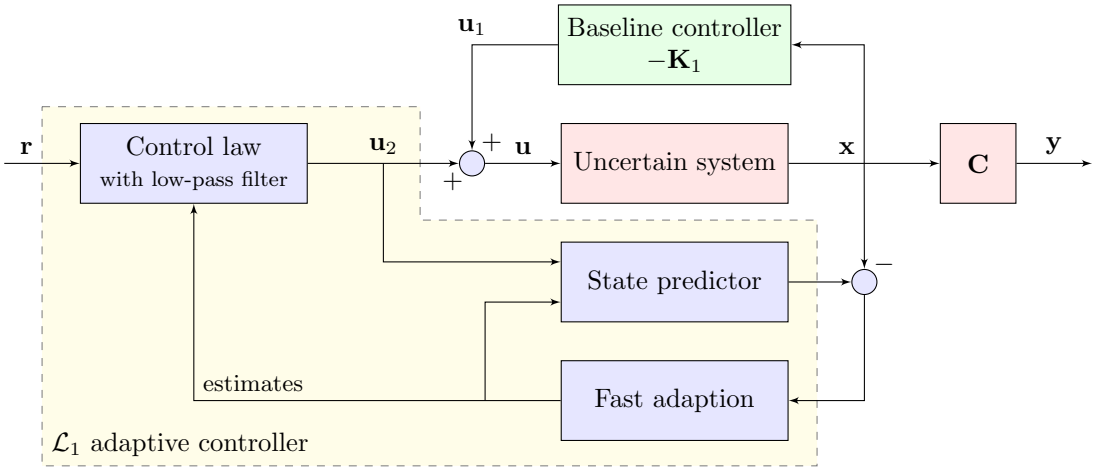

Figure 3: $\mathcal{L}_1$ Adaptive Control Architecture

where $\mathbf{B}_{um} \in \mathbb{R}^{n\times(n-m)}$ is a constant matrix such that $\mathbf{B}_m^T\mathbf{B}_{um} = 0$ and $[\mathbf{B}_m\ \mathbf{B}_{um}]$ has rank n so that

$$\begin{bmatrix}\mathbf{f}_1(t,\mathbf{x}(t))\\ \mathbf{f}_2(t,\mathbf{x}(t))\end{bmatrix} = \begin{bmatrix}\mathbf{B}_m & \mathbf{B}_{um}\end{bmatrix}^{-1}\tilde{\mathbf{f}}(t,\mathbf{x}(t)) \tag{28}$$

We define the following state predictor [Hovakimyan and Cao, 2010, pp 144]

$$\dot{\hat{\mathbf{x}}}(t) = \mathbf{A}_m\hat{\mathbf{x}}(t) + \mathbf{B}_m\left(\hat{\mathbf{\Delta}}\mathbf{u}(t) + \hat{\boldsymbol{\eta}}_1\right) + \mathbf{B}_{um}\hat{\boldsymbol{\eta}}_2 \tag{29}$$

where $\hat{\mathbf{x}}(t)$ is the state of the predictor, $\hat{\mathbf{\Delta}}$ is the estimated uncertain input gain matrix and $\hat{\boldsymbol{\eta}}_i = \hat{\boldsymbol{\theta}}_i\|\mathbf{x}(t)\|_{\mathcal{L}_\infty,t}$ $+\hat{\boldsymbol{\sigma}}_i$, $i = 1, 2$ where $\hat{\boldsymbol{\theta}}_i(t)$ and $\hat{\boldsymbol{\sigma}}_i$ are vectors of the estimated parameters and

$$\|\mathbf{x}(t)\|_{\mathcal{L}_\infty,t} := \max_{0\le\tau\le t}\left(\max_{i=1,\ldots,n}|x_i(\tau)|\right) \tag{30}$$

is the $\mathcal{L}_\infty$-norm of the state, $\mathbf{x}$, over all time prior to the current time, t.

The following adaption laws are defined for the estimated variables

$$\dot{\hat{\mathbf{\Delta}}}(t) = \Gamma\,\mathrm{proj}\left(\hat{\mathbf{\Delta}}(t), -(\tilde{\mathbf{x}}^T(t)\mathbf{P}\mathbf{B}_m)^T\mathbf{u}^T(t)\right) \tag{31}$$

$$\dot{\hat{\boldsymbol{\theta}}}_1(t) = \Gamma\,\mathrm{proj}\left(\hat{\boldsymbol{\theta}}_1(t), -(\tilde{\mathbf{x}}^T(t)\mathbf{P}\mathbf{B}_m)^T\|\mathbf{x}(t)\|_{\mathcal{L}_\infty,t}\right) \tag{32}$$

$$\dot{\hat{\boldsymbol{\sigma}}}_1(t) = \Gamma\,\mathrm{proj}\left(\hat{\boldsymbol{\sigma}}_1(t), -(\tilde{\mathbf{x}}^T(t)\mathbf{P}\mathbf{B}_m)^T\right) \tag{33}$$

$$\dot{\hat{\boldsymbol{\theta}}}_2(t) = \Gamma\,\mathrm{proj}\left(\hat{\boldsymbol{\theta}}_2(t), -(\tilde{\mathbf{x}}^T(t)\mathbf{P}\mathbf{B}_{um})^T\|\mathbf{x}(t)\|_{\mathcal{L}_\infty,t}\right) \tag{34}$$

$$\dot{\hat{\boldsymbol{\sigma}}}_2(t) = \Gamma\,\mathrm{proj}\left(\hat{\boldsymbol{\sigma}}_2(t), -(\tilde{\mathbf{x}}^T(t)\mathbf{P}\mathbf{B}_{um})^T\right) \tag{35}$$

where $\tilde{\mathbf{x}}(t) = \hat{\mathbf{x}}(t) - \mathbf{x}(t)$ is the predictor error, $\Gamma \in \mathbb{R}_+$ is the adaption gain, $\mathbf{P}$ is the solution to the algebraic Lyapunov equation ${\mathbf{A}_m}^T\mathbf{P} + \mathbf{P}\mathbf{A}_m = -\mathbf{Q}$ for $\mathbf{Q} = \mathbf{Q}^T > 1$ and $\mathbf{P} = \mathbf{P}^T > 0$ and $\mathrm{proj}(\cdot,\cdot)$ denotes the projection operator defined in Appendix A. The projection operator ensures that the estimates remain within allotted bounds.

The following are required for the subsequent definition of the adaptive control law:

$$\begin{bmatrix}\mathbf{H}_{xm}(s)\\ \mathbf{H}_{xum}(s)\end{bmatrix} = (sI - \mathbf{A}_m)^{-1}\begin{bmatrix}\mathbf{B}_m\\ \mathbf{B}_{um}\end{bmatrix}, \tag{36}$$

$$\begin{bmatrix}\mathbf{H}_m(s)\\ \mathbf{H}_{um}(s)\end{bmatrix} = \mathbf{C}\begin{bmatrix}\mathbf{H}_{xm}(s)\\ \mathbf{H}_{xum}(s)\end{bmatrix}. \tag{37}$$

The linear control law is given in the Laplace domain by

$$\mathbf{u}_2(s) = -\mathbf{K}_2\mathbf{H}_D(s)\hat{\boldsymbol{\eta}}(s) \tag{38}$$

where $\mathbf{K}_2 \in \mathbb{R}^{m\times m}$ is a feedback gain matrix, $\mathbf{H}_D(s)$ is an $m \times m$ strictly proper transfer function matrix, $\hat{\boldsymbol{\eta}}(s)$ is the Laplace transform of $\hat{\boldsymbol{\eta}}(t)$ which is

$$\hat{\boldsymbol{\eta}}(t) = \mathbf{K}_g\mathbf{r}(t) - \left(\hat{\boldsymbol{\Delta}}\mathbf{u}_2(t) + \hat{\boldsymbol{\eta}}_1(t) + \hat{\boldsymbol{\eta}}_{2m}(t)\right) \tag{39}$$

where $\mathbf{r}(t)$ is the reference input, $\hat{\boldsymbol{\eta}}_{2m}(t)$ is the inverse Laplace transform of the signal

$$\hat{\boldsymbol{\eta}}_{2m}(s) = \mathbf{H}_m(s)^{-1}\mathbf{H}_{um}(s)\hat{\boldsymbol{\eta}}_2(s), \tag{40}$$

and $\mathbf{K}_g$ ensures the system output tracks the reference signal in the steady state. Transfer function matrix $\mathbf{H}_D(s)$ leads to a strictly proper stable low pass filter matrix, $\mathbf{H}_C(s)$, with $\mathbf{H}_C(0) = I$. A block diagram of the arrangement is shown in Figure 4. The transfer function matrix, $\mathbf{H}_C(s)$, is

$$\mathbf{H}_C(s) = \boldsymbol{\Delta}\mathbf{K}_2\mathbf{H}_D(s)\left(I + \boldsymbol{\Delta}\mathbf{K}_2\mathbf{H}_D(s)\right)^{-1}. \tag{41}$$

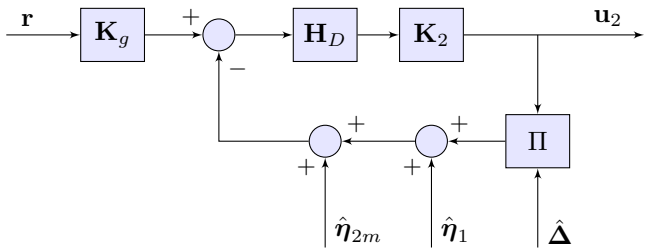

Figure 4: Low Pass Filter for $\mathcal{L}_1$ Adaptive Controller

4 Controller Design

4.1 LQR Inner-loop Controller

An LQR controller is designed as the inner-loop stabilizing controller, $\mathbf{K}_1$, described in Section 3.1. A standard formulation is used [Stevens and Lewis, 2003, e.g.]. That is, for a linear system $\dot{\mathbf{x}}(t) = \mathbf{A}\mathbf{x}(t)+\mathbf{B}\mathbf{u}(t)$, the control that minimizes the quadratic cost function

$$J = \int_0^\infty \left(\mathbf{x}^T\mathbf{Q}\mathbf{x}(t) + \mathbf{u}^T(t)\mathbf{R}\mathbf{u}(t)\right)dt \tag{42}$$

where $\mathbf{Q}$ and $\mathbf{R}$ are weighting matrices, is given by $\mathbf{u}(t) = -\mathbf{K}\mathbf{x}(t)$, with

$$\mathbf{K} = \mathbf{R}^{-1}\mathbf{B}^T\mathbf{P} \tag{43}$$

where $\mathbf{P} = \mathbf{P}^T \geq 0$ is the solution to

$$\mathbf{A}^T\mathbf{P} + \mathbf{P}\mathbf{A} + \mathbf{Q} - \mathbf{P}\mathbf{B}\mathbf{R}^{-1}\mathbf{B}^T\mathbf{P} = 0. \tag{44}$$

Hence $\mathbf{K}_1$ is set to this optimal controller.

A small perturbation linear model of (13) is required. Linearizing about the hover equilibrium state, $\mathbf{x}_0$ and control $\mathbf{u}_0$ gives

$$\delta\dot{\mathbf{x}} = \mathbf{A}\delta\mathbf{x} + \mathbf{B}\delta\mathbf{u} \tag{45}$$

where $\delta\mathbf{x}$ and $\delta\mathbf{u}$ represents the small perturbations of the state and control about $\mathbf{x}_0$ and $\mathbf{u}_0$ respectively, and

$$\mathbf{A} = \begin{bmatrix} 0_{1\times6} & 0_{1\times3} & 0_{1\times1} & -g & 0_{1\times1} \\ 0_{1\times6} & 0_{1\times3} & g & 0_{1\times1} & 0_{1\times1} \\ 0_{4\times6} & 0_{4\times3} & 0_{4\times1} & 0_{4\times1} & 0_{4\times1} \\ I_{6\times6} & 0_{6\times3} & 0_{6\times1} & 0_{6\times1} & 0_{6\times1} \end{bmatrix}, \tag{46}$$

$$\mathbf{B}_m = \begin{bmatrix} 0_{2\times1} & 0_{5\times3} \\ -1/m & 0_{1\times3} \\ 0_{3\times1} & 0_{3\times3} \\ 0_{3\times1} & \mathbf{I}^{-1} \end{bmatrix}, \tag{47}$$

and

$$\mathbf{u}_0 = \begin{bmatrix} {v_h}^2 & {v_h}^2 & {v_h}^2 & {v_h}^2 \end{bmatrix}^T \tag{48}$$

where

$$v_h = \sqrt{(mg)/(4k_f)} \tag{49}$$

is the voltage for each actuator required for hover condition. Hence we define $\mathbf{u} = \mathbf{U} - \mathbf{u}_0$.

The weighting matrices are chosen to be $\mathbf{Q} = 100I$ and $\mathbf{R} = I$. The resulting inner-loop controller is

$$\mathbf{K}_1 = \begin{bmatrix} -11.46 & 0 & -8.86 & 0 & 14.9 & 6.27 & -7.07 & 0 & -5.0 & 0 & 56.5 & 5.0 \\ 0 & -11.46 & -8.86 & -14.9 & 0 & -6.27 & 0 & -7.07 & -5.0 & -56.5 & 0 & -5.0 \\ 11.46 & 0 & -8.86 & 0 & 0 & 6.27 & 7.07 & 0 & -5.0 & 0 & -56.5 & 5.0 \\ 0 & 11.46 & -8.86 & 14.9 & 14.9 & -6.27 & 0 & 7.07 & -5.0 & 56.5 & 0 & -5.0 \end{bmatrix}. \tag{50}$$

4.2 $\mathcal{L}_1$ adaptive controller design

Design of the state predictor, (29), is considered first. The $\mathcal{L}_1$ adaptive controller is applied to a system of the form in (25). Considering the system (22), we can obtain a model of $\mathbf{f}(t, \mathbf{x})$ by subtracting the linear model (45) from the nonlinear model (13) giving

$$\mathbf{f}(\mathbf{x}) = \begin{bmatrix} (\theta - s_\theta)g - (QW - RV) \\ (c_\theta s_\phi - \phi)g - (RU - PW) \\ (c_\theta c_\phi - 1)g - (PV - QU) \\ -\left((I_z - I_y)/I_x\right)QR \\ -\left((I_x - I_z)/I_y\right)RP \\ -\left((I_y - I_x)/I_z\right)PQ \\ (c_\psi c_\theta - 1)U + (c_\psi s_\theta s_\phi - s_\psi c_\phi)V + (c_\psi s_\theta c_\phi + s_\psi s_\phi)W \\ (s_\psi c_\theta)U + (s_\psi s_\theta s_\phi + c_\psi c_\phi - 1)V + (s_\psi s_\theta c_\phi - c_\psi s_\phi)W \\ -s_\theta U + (c_\theta s_\phi)V + (c_\theta c_\phi - 1)W \\ (t_\theta s_\phi)Q + (t_\theta c_\phi)R \\ (c_\phi - 1)Q - s_\phi R \\ (s_\phi/c_\psi)\,Q + (c_\phi/c_\theta - 1)\,R \end{bmatrix} \tag{51}$$

To simplify the calculations, we assume that $\mathbf{\Delta} = I$, hence $\hat{\mathbf{f}} = \mathbf{f}$ and factor the unknown nonlinear part $\mathbf{f}(t, \mathbf{x}(t))$ into matched component of unknown nonlinearity, $\mathbf{f}_1(t, \mathbf{x}(t))$ and unmatched uncertainties, $\mathbf{f}_2(t, \mathbf{x}(t))$ as in (27) with $\mathbf{B}_m$ from (47) and

$$\mathbf{B}_{um} = \begin{bmatrix} I_2 & 0_{2\times6} \\ 0_{4\times2} & 0_{4\times6} \\ 0_{6\times2} & I_6 \end{bmatrix} \tag{52}$$

so that the required conditions that $\mathbf{B}_m^T\mathbf{B}_{um} = 0$ and $[\mathbf{B}_m\ \mathbf{B}_{um}]$ has rank 12 are both satisfied.

The adaption gain for the variable estimation in the adaptation laws, (31) is set to $\Gamma = 1000$, whilst $\mathbf{P} \in \mathbb{R}^{12\times12}$ is calculated from the algebraic Lyapunov equation with $\mathbf{Q} = I_{12}$. The bounds of the estimator

parameters are chosen conservatively by trial and error, which the $L_{1\rho_r} = 40$, $B_{10} = 10$, $L_{1\rho_r} = 2$ and $B_{20} = 1$, thus

$$\hat{\beta}_1 \in [-40, 40]I_4, \qquad \hat{\sigma}_1 \in [-10, 10]I_4, \tag{53}$$

$$\hat{\beta}_2 \in [-2, 2]I_8, \qquad \hat{\sigma}_1 \in [-10, 10]I_8. \tag{54}$$

The bound for uncertain gain matrix estimator is defined as

$$\hat{\mathbf{\Delta}} = \begin{bmatrix} \hat{\delta}_1 & 0 & 0 & 0 \\ 0 & \hat{\delta}_2 & 0 & 0 \\ 0 & 0 & \hat{\delta}_3 & 0 \\ 0 & 0 & 0 & \hat{\delta}_4 \end{bmatrix}, \quad \hat{\delta}_i \in (0, 1], i = 1, 2, 3, 4. \tag{55}$$

For the low pass filter design, $\mathbf{H}_D(s)$ is simply chosen to be $\mathbf{H}_D(s) = \frac{1}{s} I_4$, this leads to the low pass filter matrix $\mathbf{H}_C(s) = \mathbf{\Delta K}(sI_m + \mathbf{\Delta K})^{-1}$. The feedback gain matrix, $\mathbf{K}$, is set to a $\mathbf{K} = kI_4$

The output of the state space system is chosen to be the physical location and the yaw angle. The yaw angle is used, because of in such a mission like surveillance, the camera direction is depends on the yaw angle. The output of the system is chosen to be the vehicle position in the earth axes, and the yaw angle, i.e. $\mathbf{y} = \begin{bmatrix} X & Y & Z & \psi \end{bmatrix}^T$ and since $\mathbf{y} = \mathbf{Cx}$, the output matrix $\mathbf{C}$ is

$$\mathbf{C} = \begin{bmatrix} 0_{3\times 6} & I_3 & 0_{3\times 2} & 0_{3\times 1} \\ 0_{1\times 6} & 0_{1\times 3} & 0_{1\times 2} & 1 \end{bmatrix}. \tag{56}$$

Finally, $\mathbf{K}_g = -(\mathbf{C}(\mathbf{A} - \mathbf{BK}_m)^{-1}\mathbf{B})^{-1}$, which ensures that the output $\mathbf{y}(t)$ tracks the reference $\mathbf{r}(t)$ at steady state.

4.3 LQR+I Controller

The $\mathcal{L}_1$ controller design is characterized by an integrating block in the $\mathbf{H}_D(s)$ element along with the inner-loop LQR controller. To test the adaptive properties of the $\mathcal{L}_1$ controller, an LQR+I controller is designed for comparative purposes as a non-adaptive controller but with similar structure to the $\mathcal{L}_1$ controller. The LQR+I controller is an LQR optimal controller based on an augmented plant model of the system that includes integral action on the output error. The structure is shown in Figure 5.

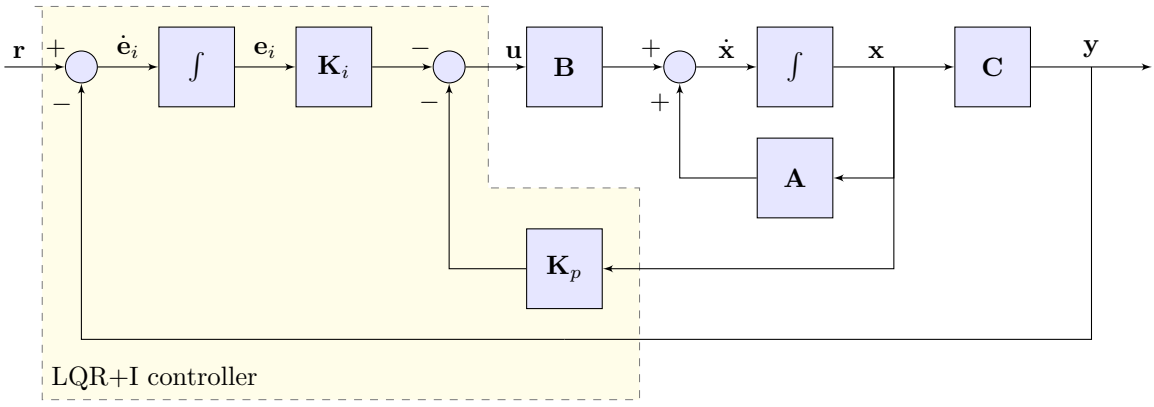

Figure 5: LQR+I Controller

To augment the plant model with integral action, define the integral of the error as

$$\mathbf{e}_i = \int_0^t (\mathbf{r} - \mathbf{y}) dt, \tag{57}$$

giving the state equation

$$\dot{\mathbf{e}}_i = \mathbf{r} - \mathbf{y}, \tag{58}$$
$$= \mathbf{r} - \mathbf{C}\mathbf{x}, \tag{59}$$

so augmenting the plant model gives

$$\begin{bmatrix} \dot{\mathbf{x}} \\ \dot{\mathbf{e}}_i \end{bmatrix} = \begin{bmatrix} \mathbf{A} & 0 \\ -\mathbf{C} & 0 \end{bmatrix} \begin{bmatrix} \mathbf{x} \\ \mathbf{e}_i \end{bmatrix} + \begin{bmatrix} \mathbf{B} \\ 0 \end{bmatrix} u + \begin{bmatrix} 0 \\ I \end{bmatrix} r \tag{60}$$

with state feedback

$$\mathbf{u} = \begin{bmatrix} -\mathbf{K}_p & -\mathbf{K}_i \end{bmatrix} \begin{bmatrix} \mathbf{x} \\ \mathbf{e}_i \end{bmatrix}, \tag{61}$$
$$= -\mathbf{K}_p\mathbf{x} - \mathbf{K}_i\mathbf{e}_i. \tag{62}$$

The controller $\begin{bmatrix} -\mathbf{K}_p & \mathbf{K}_i \end{bmatrix}$ is designed using the LQR method described in Section 4.1. The weighting matrices are chosen to be $\mathbf{Q} = \text{diag}([100I_{12}, 1000I_4])$ and $\mathbf{R} = I_4$.

5 Simulations

The model and controller are tested in simulation for the recovery performance to partial failures in the actuators/effectors. The failures are assumed to be a partial loss of input voltage that results in an instantaneous decrease in the thrust of a rotor. It is assumed that a voltage loss also results in a loss of the maximum voltage supplied to a motor. The maximum voltage is 14.8 V. From (49), to maintain hover a faulty voltage supply must be able to supply $v_h = 7.28$ V. Mapping this value to the failure model given by (20) gives a range, $\delta_i \in (0.2420, 1.0]$.

Figure 6 shows the failure free transient response for both the LQR+I and $\mathcal{L}_1$ controllers to a 1.0 m step demand change simultaneously in both the X and Y positions. The performances are fairly comparable, with a slightly faster response for the LQR+I controller at the expense of some additional altitude undershoot and yaw deviation. The applied voltages are shown in Figure 7.

5.1 Failure at hover

The first test case considers the upset from hover of an instantaneous failure in $i = 1$ motor voltage supply occurring at $t = 1$ second, that is

$$\delta_1(t) = \begin{cases} 1.0 \text{ for } 0 \leq t < 1.0 \\ \tilde{\delta}_1 \text{ for } 1.0 \leq t \end{cases} \tag{63}$$

and $\delta_i(t) = 1.0$ for $i = 2, 3, 4$.

For the LQR+I controller, simulation results for $\tilde{\delta}_1 = \{0.35, 0.4, 0.6, 0.8\}$ are presented in Figure 8. The vehicle is at steady state hover until $t = 1.0$ s. When the voltage supply fault occurs, rotor 1 loses some thrust and there is a subsequent loss of altitude. It also generates a pitch moment with a resulting displacement in the X position. The dynamic coupling also causes a smaller roll moment and a displacement in the Y position. The change in rotation rate of rotor 1 also causes a yaw moment and resulting yaw rotation. Values of $\tilde{\delta}_1 \lesssim 0.34$ result in an unstable response, the reason is that the reduced maximum supply voltage results in a saturated motor demand. For $\tilde{\delta}_1 = 0.35$, the reduced maximum supply voltage is 8.76 V, which, from Figure 9, is reached for a short time between 4 and 5 seconds.

For the $\mathcal{L}_1$ adaptive controller, simulation results for $\tilde{\delta}_1 = \{0.3, 0.4, 0.6, 0.8\}$ are presented in Figure 10. Values of $\tilde{\delta}_1 \lesssim 0.27$ result in an unstable response for the same reason that the reduced maximum supply voltage results in a saturated motor demand. This can be seen in Figure 11 for $\tilde{\delta}_1 = 0.3$. From the plots, it is clear that the $\mathcal{L}_1$ adaptive controller has a better performance, with reduced deviations from hover and faster response. In addition it has a greater range of $\tilde{\delta}_1$ for which the system remains stable.

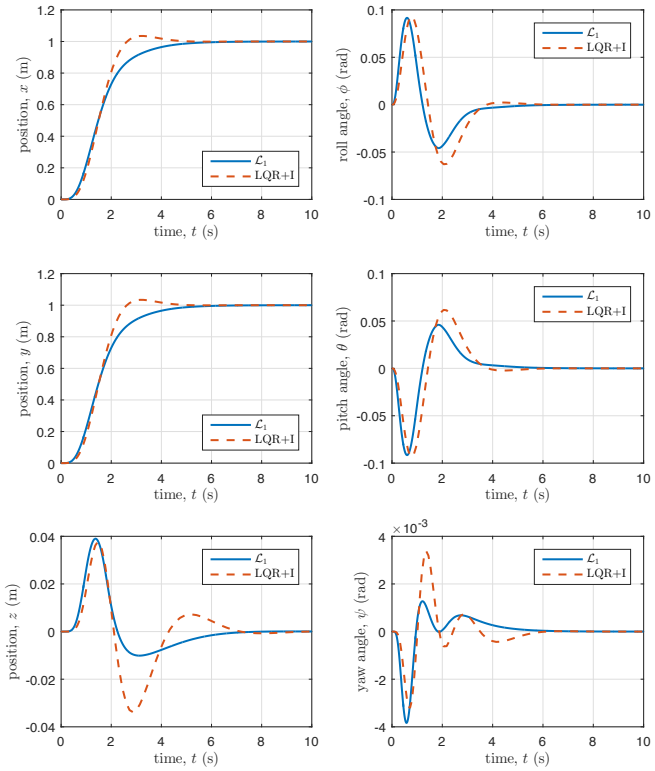

Figure 6: Response to unit demand in X and Y positions – failure free case

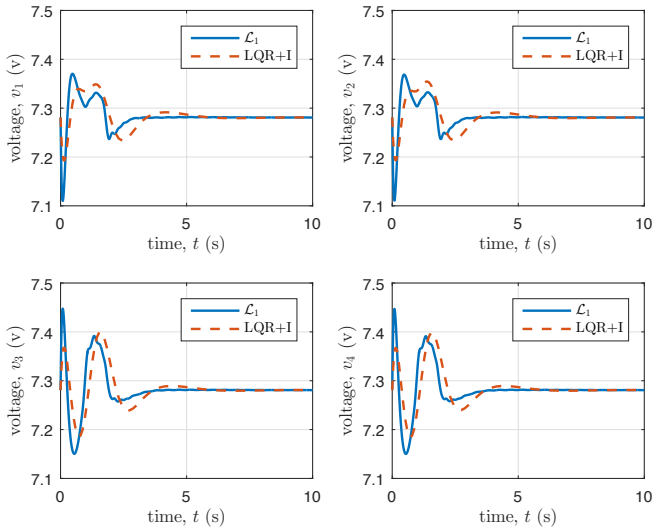

Figure 7: The voltage input for each rotor in response to a unit demand in X and Y positions – failure free case

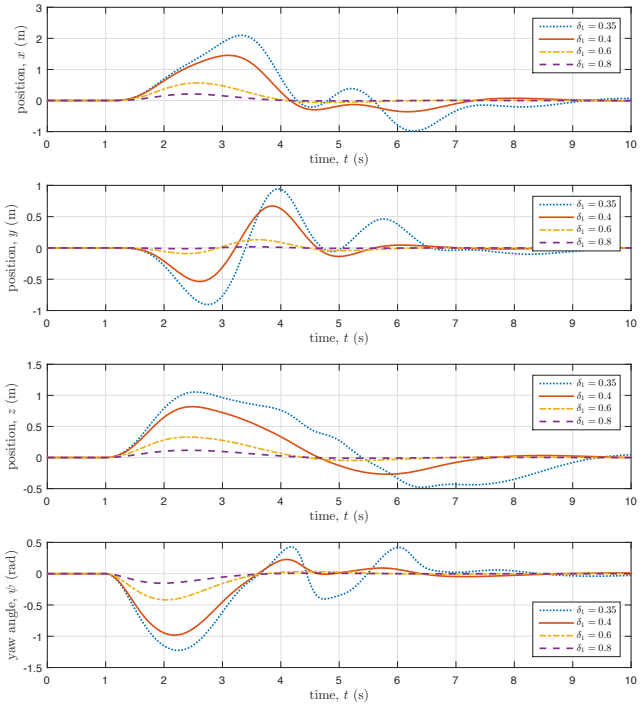

Figure 8: Output $\mathbf{y}(t)$ for Rotor 1 losses of thrust – LQR+I controller

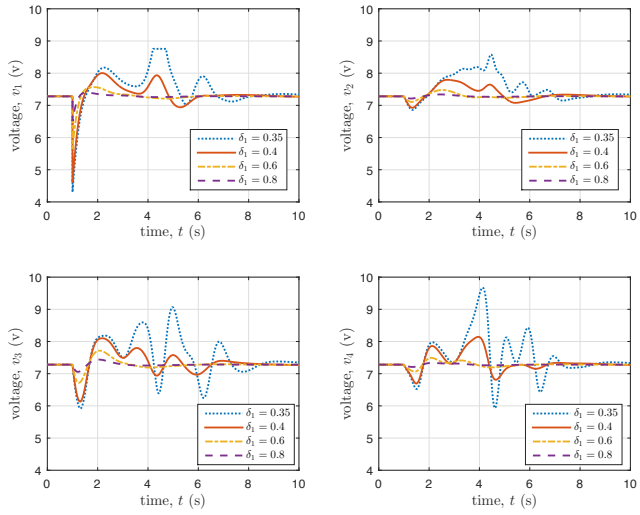

Figure 9: The voltage input for each rotor for Rotor 1 losses of thrust – LQR+I controller

5.2 Failure during transient

The second test case considers an intermittent failure during a manoeuvre responding to a 1.0 m step change demand simultaneously in both the X and Y positions. The failure model in $i = 2$ motor voltage is

$$\delta_2(t) = \begin{cases} 1.0 \text{ for } 0 \leq t < 1.0 \\ 0.5 \text{ for } 1.0 \leq t < 3.0 \\ 1.0 \text{ for } 3.0 \leq t \end{cases} \tag{64}$$

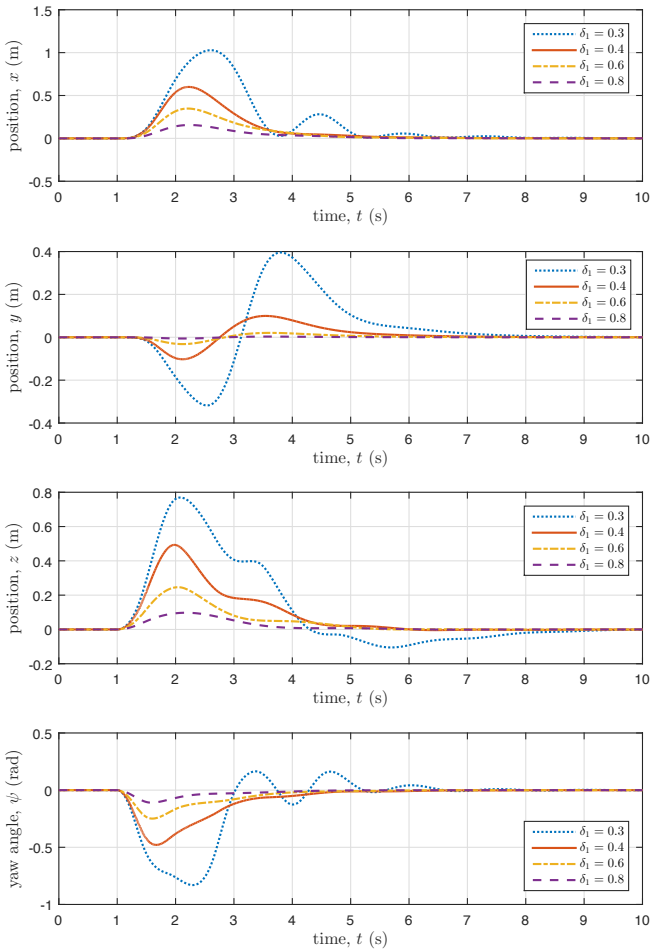

Figure 10: Output $\mathbf{y}(t)$ for Rotor 1 losses of thrust – $\mathcal{L}_1$ controller

and $\delta_i(t) = 1.0$ for $i = 1, 3, 4$.

The responses shown in Figure 12 clearly show that the $\mathcal{L}_1$ controller is better able to cope with the intermittent failure, with a less oscillatory response and smaller deviations. Figure 13 shows that this better performance is achieved by the adaptation to the failure in the voltage supply to rotor 2 by demanding a greater voltage to that rotor.

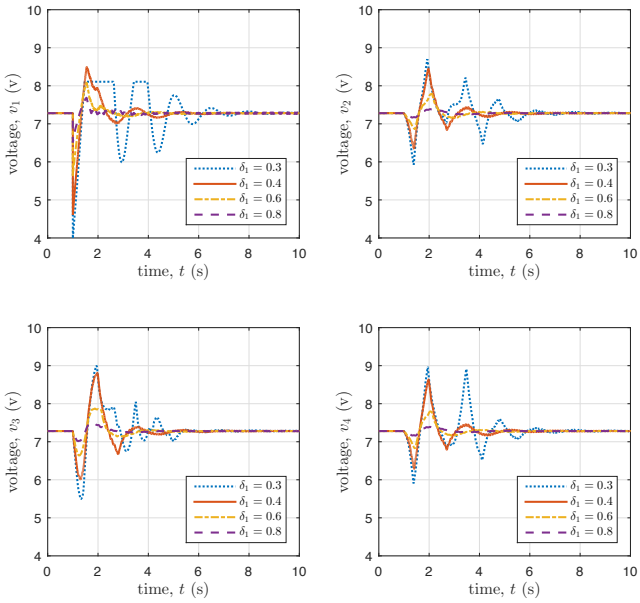

Figure 11: The voltage input for each rotor for Rotor 1 losses of thrust – $\mathcal{L}_1$ controller

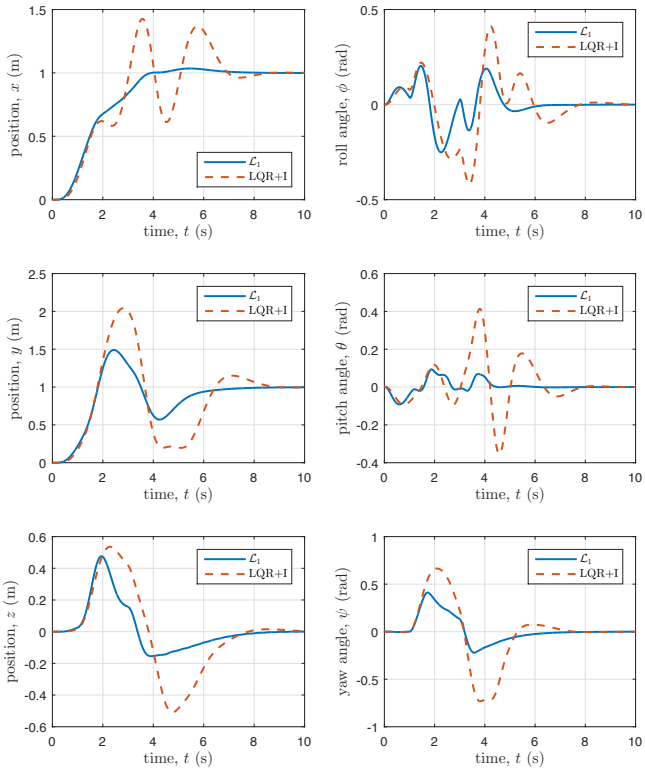

Figure 12: Response to unit demand in X and Y positions – intermittent failure case

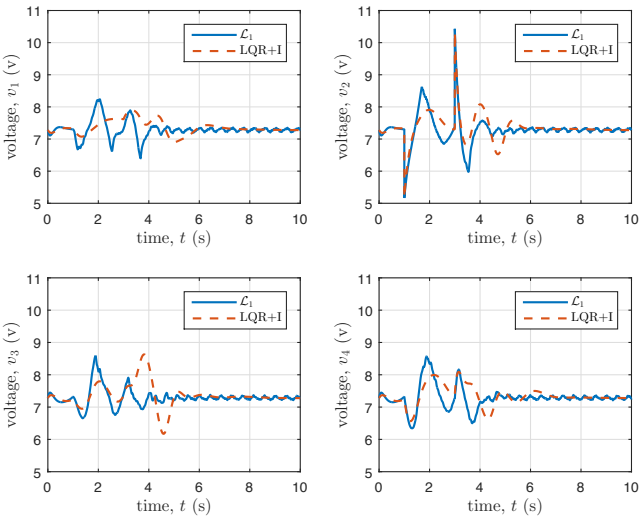

Figure 13: The voltage input for each rotor – intermittent failure case

6 Conclusions

This paper investigates the performance of an $\mathcal{L}_1$ adaptive controller for the fault tolerant control of a quadrotor. The proposed scheme uses an LQR controller to stabilize the vehicle in an inner loop, the $\mathcal{L}_1$ adaptive controller is applied in the outer loop to estimate and compensate for the actuator uncertainty resulting from failures. Whilst some conditions for the stability of non-linear systems subject to uncertainty have been established for $\mathcal{L}_1$ adaptive controllers [Hovakimyan and Cao, 2010], in practice these are rather hard to determine except for trivial systems. A trial and error approach was hence used to design the controller. The simulations show the adaptive properties of the controller to partial failures in the voltage supply to the motors, and show the better performance of the $\mathcal{L}_1$ adaptive controller compared to an LQG controller with a similar structure and closed loop performance under non-failure conditions.

Although quadrotors cannot tolerate total failure of a rotor without loss of control of one of the degrees of freedom, applying the $\mathcal{L}_1$ adaptive controller to a hexrotor or octorotor would increase the reliability of such vehicles without recourse to methods that require fault detection schemes and control reallocation [Marks et al., 2012, Hamayun et al., 2015, for example].

The control scheme is tested in simulation of a simple model that ignores aerodynamic and gyroscopic effects. Hence for further work, testing with a fuller model [Martínez, 2007] is recommended followed by implementation on an actual platform and flight test. The effect of sensor noise should also be considered along with investigation into the influence of wind disturbances and tolerance to sensor failures. Furthermore, performance at other flight conditions such as steady forward flight should be investigated. The consequence of the loss of a complete effector and the subsequent loss of control of a degree-of-freedom also needs exploring. The question of whether this scheme can be extended to maintain control over fewer degreees-of-freedom in a similar manner to Mueller and D'Andrea [2015] is an open one.

References

V. G. Adîr, A. M. Stoica, A. Marks, and J. F. Whidborne. Modelling, stabilization and single motor failure recovery of a 4Y octorotor. In *Proc. 13th IASTED International Conference on Intelligent Systems and Control (ISC 2011)*, pages 82–87, Cambridge, U.K., July 2011. doi: 10.2316/P.2011.744-070.

V. S. Akkinapalli, G. P. Falconí, and F. Holzapfel. Attitude control of a multicopter using $\mathcal{L}_1$ augmented quaternion based backstepping. In *2014 IEEE International Conference on Aerospace Electronics and Remote Sensing Technology (ICARES 2014)*, pages 170–178, Yogyakarta, Indonesia, November 2014. doi: 10.1109/ICARES.2014.7024376.

H. Alwi and C. Edwards. Sliding mode fault-tolerant control of an octorotor using linear parameter varying-based schemes. *IET Proc. Control Theory and Appl.*, 9:618–636, 2015. ISSN 1751-8644. doi: 10.1049/iet-cta.2014.0215.

A. Bouabdallah, A. Noth, and R. Siegwart. PID vs LQ control techniques applied to an indoor micro quadrotor. In *Proc. IEEE Conf. on Intel. Robot. Systems*, Sendai, Japan, September 2004a. doi: 10.1109/IROS.2004.1389776.

S. Bouabdallah, P. Murrieri, and R. Siegwart. Design and control of an indoor micro quadrotor. In *Proc. International Conference on Robotics and Automation (ICRA2004)*, pages 4393–4398, New Orleans, LA, April 2004b. doi: 10.1109/ROBOT.2004.1302409.

C. Cao and N. Hovakimyan. Design and analysis of a novel adaptive controller, part 1: Control signal and asymptotic stability. In *Proc. 2006 American Control Conference (ACC)*, pages 3397–3402, Minneapolis, MN, 2006a. doi: 10.1109/ACC.2006.1657243.

C. Cao and N. Hovakimyan. Design and analysis of a novel adaptive controller, part 2: Guaranteed transient performance. In *Proc. 2006 American Control Conference (ACC)*, pages 3403–3408, Minneapolis, MN, 2006b. doi: 10.1109/ACC.2006.1657244.

C. Cao and N. Hovakimyan. $\mathcal{L}_1$ adaptive output feedback controller for systems with time-varying unknown parameters and bounded disturbances. In *Proc. 2007 American Control Conference (ACC)*, pages 486–491, New York, NY, July 2007a. doi: 10.1109/ACC.2007.4282994.

C. Cao and N. Hovakimyan. Guaranteed transient performance with $\mathcal{L}_1$ adaptive controller for systems with unknown time-varying parameters and bounded disturbances: Part i. In *Proc. 2007 American Control Conference (ACC)*, pages 3925–3930, New York, NY, July 2007b. doi: 10.1109/ACC.2007.4282485.

C. Cao and N. Hovakimyan. Stability margins of $\mathcal{L}_1$ adaptive controller: Part II. In *Proc. 2007 American Control Conference (ACC)*, pages 3931–3936, New York, NY, July 2007c. doi: 10.1109/ACC.2007.4282486.

C. Cao and N. Hovakimyan. $\mathcal{L}_1$ adaptive controller for multi-input multi-output systems in the presence of unmatched disturbances. In *Proc. 2008 American Control Conference (ACC)*, pages 4105–4110, Seattle, WA, June 2008a. doi: 10.1109/ACC.2008.4587136.

C. Cao and N. Hovakimyan. $\mathcal{L}_1$ adaptive controller for systems with unknown time-varying parameters and disturbances in the presence of non-zero trajectory initialization error. *Int. J. Control*, 81(7):1148–1162, 2008b. doi: 10.1080/00207170701670939.

C. Cao and N. Hovakimyan. Design and analysis of a novel $\mathcal{L}_1$ adaptive control architecture with guaranteed transient performance. *IEEE Trans. Autom. Control*, 53(2):586–591, 2008c. ISSN 0018-9286. doi: 10.1109/TAC.2007.914282.

C. Cao and N. Hovakimyan. $\mathcal{L}_1$ adaptive output feedback controller for non-strictly positive real reference systems: Missile longitudinal autopilot design. *J. Guid. Control Dyn.*, 32(3):717–726, 2009. ISSN 0018-9286. doi: 10.2514/1.40877.

E. Capello, A. Scola, G. Guglieri, and F. Quagliotti. Mini quadrotor UAV: Design and experiment. *J. Aerosp. Eng.*, 25(4):559–573, 2012. doi: 10.1061/(ASCE)AS.1943-5525.0000171.

E. Capello, F. Quagliotti, and R. Tempo. Randomized approaches and adaptive control for quadrotor UAVs. In *2013 International Conference on Unmanned Aircraft Systems (ICUAS)*, pages 461–470, Atlanta, GA, May 2013. doi: 10.1109/ICUAS.2013.6564721.

A. Chamseddine, D. Theilliol, Y.M. Zhang, C. Join, and C. A. Rabbath. Active fault-tolerant control system design with trajectory re-planning against actuator faults and saturation: Application to a quadrotor unmanned aerial vehicle. *Int. J. Adapt. Control Signal Process.*, 29(1):1–23, 2015. doi: 10.1002/acs.2451.

M. V. Cook. *Flight Dynamics Principles*. Elsevier, Oxford, UK, 3rd edition, 2013.

I. D. Cowling, J. F. Whidborne, and A. K. Cooke. Optimal trajectory planning and LQR control for a quadrotor UAV. In *Proc. UKACC Int. Conf. Control 2006 (ICC2006)*, page CD ROM paper 125, Glasgow, UK, September 2006.

I. D. Cowling, O. A. Yakimenko, J. F. Whidborne, and A. K. Cooke. Direct method based control system for an autonomous quadrotor. *J. Intell. Robotic Syst.*, 60(2):285 –316, 2010. doi: 10.1007/s10846-010-9416-9.

P. De Monte and B. Lohmann. Position trajectory tracking of a quadrotor helicopter based on L_1 adaptive control. In *Proc. 2013 European Control Conference (ECC)*, pages 3346–3353, Zurich, Switzerland, July 2013.

P. De Monte and B. Lohmann. Position trajectory tracking of a quadrotor based on L1 adaptive control. *Automatisierungstechnik*, 62(3):188–202, 2014. doi: 10.1515/auto-2013-1035.

Z. T. Dydek, A. M. Annaswamy, and E. Lavretsky. Adaptive control of quadrotor UAVs: A design trade study with flight evaluations. *IEEE Trans. Contr. Syst. Technol.*, 21(4):1400–1406, 2013. doi: 10.1109/TCST.2012.2200104.

C. Ene, A.-M. Stoica, and J. F. Whidborne. Application of L_1 adaptive controller to longitudinal dynamics of a high manoeuvrability aircraft. In *19th IFAC Symposium on Automatic Control in Aerospace (ACA 2013)*, pages 447–452, Würzburg, Germany, September 2013. doi: 10.3182/20130902-5-DE-2040.00133.

M. T. Hamayun, C. Edwards, H. Alwi, and A. Bajodah. A fault tolerant direct control allocation scheme with integral sliding modes. *International Journal of Applied Mathematics and Computer Science*, 25(1): 93–102, 2015. doi: 10.1515/amcs-2015-0007.

N. Hovakimyan and C. Cao. $\mathcal{L}_1$ *Adaptive Control Theory: Guaranteed Robustness with Fast Adaptation*. Advances in Design and Control. SIAM, Philadelphia, PA, 2010.

A. Lanzon, A. Freddi, and S. Longhi. Flight control of a quadrotor vehicle subsequent to a rotor failure. *J. Guid. Control Dynam.*, 37(2):580–591, 2014. doi: 10.2514/1.59869.

S. Mallikarjunan, B. Nesbitt, E. Kharisov, E. Xargay, C. Cao, and N. Hovakimyan. $\mathcal{L}_1$ adaptive controller for attitude control of multirotors. In *Proc. AIAA Guidance, Navigation, and Control Conference*, Minneapolis, MN, August 2012. doi: 10.2514/6.2012-4831.

A. Marks, J. F. Whidborne, and I. Yamamoto. Control allocation for fault tolerant control of a VTOL octorotor. In *UKACC International Conference on Control 2012*, pages 357 – 362, Cardiff, U.K., September 2012. doi: 10.1109/CONTROL.2012.6334656.

V. M. Martínez. Modelling of the flight dynamics of a quadrotor helicopter. MSc dissertation, Cranfield University, Bedfordshire, U.K., 2007.

A. A. Mian and D. Wang. Nonlinear flight control strategy for an underactuated quadrotor aerial robot. In *Proc. IEEE International Conference on Networking, Sensing and Control (ICNSC 2008)*, pages 938–942, Sanya, China, April 2008. doi: 10.1109/ICNSC.2008.4525351.

B. Michini and J. How. $\mathcal{L}_1$ adaptive control for indoor autonomous vehicles: Design process and flight testing. In *Proc. AIAA Guidance, Navigation and Control Conference*, number AIAA-2009-5754, Chicago, IL, August 2009. doi: 10.2514/6.2009-5754.

B. Michini, J. Redding, N. K. Ure, M. Cutler, and J. P. How. Design and flight testing of an autonomous variable-pitch quadrotor. In *Proc. 2011 IEEE International Conference on Robotics and Automation (ICRA 2011)*, pages 2978–2979, Shanghai, China, May 2011. doi: 10.1109/ICRA.2011.5980561.

M. W. Mueller and R. D'Andrea. Stability and control of a quadrocopter despite the complete loss of one, two, or three propellers. In *IEEE International Conference on Robotics and Automation (ICRA)*, pages 45–52, Hong Kong, May 2014. doi: 10.1109/ICRA.2014.6906588.

M. W. Mueller and R. D'Andrea. Relaxed hover solutions for multicopters: application to algorithmic redundancy and novel vehicles. *International Journal of Robotics Research*, 2015. To appear.

F. Rinaldi, S. Chiesa, and F. Quagliotti. Linear quadratic control for quadrotors UAVs dynamics and formation flight. *J. Intell. Robotic Syst.*, 70(1-4):203–220, 2013. ISSN 0921-0296. doi: 10.1007/s10846-012-9708-3.

D. Rotondo, F. Nejjari, and V. Puig. Robust quasi-LPV model reference FTC of a quadrotor UAV subject to actuator faults. *Int. J. Appl. Math. Comput. Sci.*, 25(1):7–22, 2015. doi: 10.1515/amcs-2015-0001.

P. Sarhadi, A. R. Noei, and A. Khosravi. L_1 adaptive pitch control of an autonomous underwater vehicle. *Int. J. Intell. Unmanned Syst.*, 2(2):107–120, 2014. doi: 10.1108/IJIUS-12-2013-0025.

B. L. Stevens and F. L. Lewis. *Aircraft Control and Simulation*. Wiley, Hoboken, NJ, 2nd edition, 2003.

A. Tayebi and S. McGilvray. Attitude stabilization of a vtol quadrotor aircraft. *IEEE Trans. Contr. Syst. Technol.*, 14(3):562–571, 2006. doi: 10.1109/TCST.2006.872519.

E. Xargay, N. Hovakimyan, and C. Cao. $\mathcal{L}_1$ adaptive controller for multi-input multi-output systems in the presence of nonlinear unmatched uncertainties. In *Proc. 2010 American Control Conference (ACC)*, pages 874–879, Baltimore, MD, June 2010. doi: 10.1109/ACC.2010.5530686.

X. Zhang and Y. Zhang. Fault-tolerant control for quadrotor UAV by employing Lyapunov-based adaptive control approach. In *AIAA Guidance, Navigation, and Control Conference*, number AIAA 2010-8052, Toronto, Canada, August 2010. doi: 10.2514/6.2010-8052.

X. Zhang, Y. Zhang, Su. C.-Y., and Y. Feng. Fault-tolerant control for quadrotor UAV via backstepping approach. In *Proc. 48th AIAA Aerospace Sciences Meeting*, number AIAA 2010-947, Orlando, FL, January 2010. doi: 10.2514/6.2010-947.

Y. Zhang and A. Chamseddine. Fault tolerant flight control techniques with application to a quadrotor UAV testbed. In T. Lombaerts, editor, *Automatic Flight Control Systems – Latest Developments*, chapter 5, pages 119–150. InTech, 2012. doi: 10.5772/38918.

Y. M. Zhang, A. Chamseddine, C. A. Rabbath, B. W. Gordon, C.-Y. Su, S. Rakheja, C. Fulford, J. Apkarian, and P. Gosselin. Development of advanced FDD and FTC techniques with application to an unmanned quadrotor helicopter testbed. *Journal of the Franklin Institute*, 350(9):2396–2422, 2013. ISSN 0016-0032. doi: 10.1016/j.jfranklin.2013.01.009.

Z. Zuo and P. Ru. Augmented $\mathcal{L}_1$ adaptive tracking control of quad-rotor unmanned aircrafts. *IEEE Trans. Aerosp. Electron. Syst.*, 50(4):3090–3101, 2014. ISSN 0018-9251. doi: 10.1109/TAES.2014.120705.

A Projection operator

The projection operator is defined as:

$$\text{proj}(\mathbf{p},\mathbf{z}) := \begin{cases} \mathbf{z} & \text{if } f(\mathbf{p}) < 0\ , \\ \mathbf{z} & \text{if } f(\mathbf{p}) \geq 0 \text{ and } \nabla f(\mathbf{p})^T\mathbf{z} \leq 0, \\ \mathbf{z} - \frac{(\nabla f)^T\mathbf{z}}{\|\nabla f\|^2}\nabla f f & \text{if } f(\mathbf{p}) \geq 0 \text{ and } \nabla f(\mathbf{p})^T\mathbf{z} > 0, \end{cases} \tag{65}$$

where $f : \mathbb{R}^n \to \mathbb{R}$ is a smooth, convex function given by

$$f(\mathbf{p}) = \frac{(\varepsilon_p + 1)\mathbf{p}^T\mathbf{p} - p_{\max}^2}{\varepsilon_p p_{\max}^2} \tag{66}$$

where $p_{\max}$ is a norm bound imposed on the vector $\mathbf{p}$, and $\varepsilon_p > 0$ is a chosen tolerance bound.

2016-01-01

Fault tolerant control of a quadrotor using L-1 adaptive control

Xu, Dan

Emerald

Xu D, Whidborne JF, Cooke A. (2016) Fault tolerant control of a quadrotor using L-1 adaptive control. International Journal of Intelligent Unmanned Systems, Volume 4, Issue 1, January 2016, pp. 43-66

http://dx.doi.org/10.1108/IJIUS-08-2015-0011